

Three-dimensional data of wire-cut surface scans under the confocal microscope (110 character maximum, inc. spaces)

Yuhang Lin^{1,2,*}, Heike Hofmann^{2,3}, Curtis Mosher⁴, Eden Amin⁵, Jeff Salyards², and Alicia Carriquiry^{1,2}

¹Iowa State University, Department of Statistics, Ames, IA, 50011, USA

²Iowa State University, Center for Statistics and Applications in Forensic Evidence, Ames, IA, 50011, USA

³University of Nebraska-Lincoln, Department of Statistics, Lincoln, NE, 68583, USA

⁴Iowa State University, Roy J Carver High Resolution Microscopy Facility, Ames, IA, 50011, USA

⁵University of Central Oklahoma, Forensic Science Institute, Edmond, OK, 73034, USA

*corresponding author(s): Yuhang Lin (yhlin@iastate.edu)

ABSTRACT

Modify later: max of 170 words: describe the study, the assay(s) performed, resulting data, and reuse potential

Wire cut data is important in forensic investigations but lacks a systematic way of analyzing the data. We created a dataset of 120 scans of aluminum wire cut in $\times 3p$ format, using 5 wire cutters and 3 locations along the 4 blades, with 2 replicates for each combination. A systematic pipeline with multiple analysis plots was developed to analyze the data and draw conclusions based on numerical measures.

Background & Summary

For forensic analysis, the investigation of marks left at crime scenes always plays an important role, and forensic examiners are particularly interested in identifying the origin of these marks, a process known as the Source Identification Problem in Forensic Science¹. For this problem, the forensic science community focuses on two different problems: **specific source problem**, where examiners aim to determine if a mark was left by a particular tool; **common source problem**, where examiners aim to determine whether two marks were left by the same tool. Currently, the accepted practice in both problems relies on visual inspection of the items under a comparison microscope. The results, according to the Theory of Identification² developed by the Association of Firearm and Toolmark Examiners (AFTE), are categorized by examiners into three types: *identification*, where the marks are believed to be made by the same source; *elimination*, where the marks are believed to be made by different tools; and *inconclusive*, where similarities or dissimilarities between marks are insufficient to allow either identification or elimination. However, this classification of types is subjective if without similarity measurements. National Research Council (NRC)³ and President's Council of Advisors on Science and Technology (PCAST)⁴ criticize the absence of objectivity and the absence of quantifiable measurements such as error rates, which highlights the need for datasets with known ground truth for conclusion validation made through similarity comparison.

In the forensic literature, Biedermann⁵ differentiates between internal and external perspectives, where the external perspective only allows general statements based on black-box studies that relate examiners' conclusions to ground truth without considering any evidence of a particular case. In order to introduce an internal perspective, there is a need for quantitative evaluation based on specific evidence. When analyzing wire-cut scan data, understanding the characteristics of toolmarks left by wire cutters becomes essential. When a blade cuts a wire, it leaves striations on the surface, as shown in Figure 1. These striations serve as evidence for similarity assessment. Though there are already cases where the evidence and testimony on wire cut play an important role in the criminal investigation and defendant conviction, no publicly available dataset currently exists for wire-cut scans, with the closest work being done by Baiker et al.⁶, which focuses on screwdrivers, not wire cutters, not to mention a standardized quantitative approach, except for visual comparisons. Thus, there is an urgent need to collect and analyze public datasets specific to wire-cut scans.

Growing research has sought to develop quantitative methods for analyzing forensic toolmarks, particularly those created by different tools. Prior studies on striated toolmarks provide some insights into key comparison factors, including angles of attack⁶, rotational axes⁷, and cutting directions⁸. There is also foundational research in forensic toolmarks emphasizing data collection and analysis, including collecting and distributing datasets for bullet and toolmark analysis^{9,10}, numerical methods



Figure 1. Microscopic close-up of striations left by a blade on the cut end of a wire.

42 for improving accuracy and consistency^{11,12}, similarity quantification techniques^{13,14}, but alignment remains a significant
43 challenge.

44 In this study, we provide a publicly available dataset of wire-cut scans, develop a systematic pipeline to analyze the data
45 quantitatively, and introduce numerical measures for similarity assessment beyond visual inspection. The dataset includes
46 multiple types of files, as summarized in Table 1.

47 To ensure full reproducibility, we describe each step in detail, including how we collected and processed the wire-cut samples
48 in [Cutting Wires](#), how we extract profiles from scanned wire cuts in [Extract Profiles](#), how we filter signals from profiles in [Filtered Signals](#), and alignment methodologies using the cross-correlation function (CCF) as similarity measurement
49 in [Align Signals](#). [Data Records](#) discusses the details regarding hosting this dataset. Technical validations of the consistency
50 of assumptions and conclusions and variability assessment are provided in [Technical Validation](#). [Usage Notes](#) includes how
51 to use our codes for signal creation, alignment, analysis, validation, and visualization, as discussed in [Methods](#) and [Technical](#)
52 [Validation](#). [Code availability](#) discusses the availability of codes for reproducibility and future research as a list. We anticipate
53 that this dataset and analysis pipeline will serve as a foundation for problems involving wire-cut evidence and be extended to
54 real-world crime scene investigations. [hyperlink location incorrect for unnumbered sections](#) it seems that the hyperlinks make
55 sure that the section is on the page

57 Methods

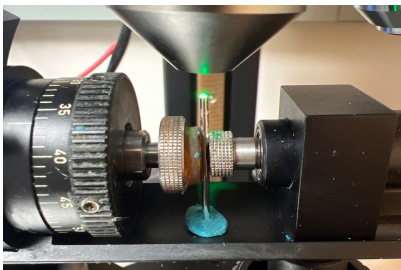
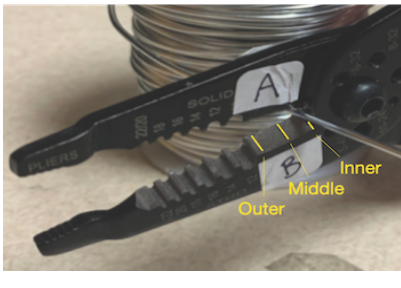
58 In this study, we use aluminum wire to create cuts. [more details: thickness, brand?](#) The physical property of aluminum wire
59 makes it an excellent candidate for keeping marks while being relatively easy to bend and non-toxic, i.e., with a hardness of
60 [XXX](#), aluminum is soft enough that tools leave marks but hard enough to not be affected by handling cut materials under the
61 microscope. In real casework, aluminum wires are not seen as often as lead or copper. We avoided using lead in the laboratory
62 setting because of its toxicity. [XXX look up the hardness value of aluminum, copper, and lead.](#)

63 Cutting Wires

64 We used 16 Gauge/1.5 mm, anodized aluminum wire to create this wire-cut dataset. In order to cut the wire, 4-inch pieces
65 were unspooled and cut using model KWS-105 Kaiweets wire cutters as shown in Figure 2a for 1 blade location, either inner,
66 middle, or outer, which gives us 1 replicate. Each piece was then cut into half to create 2-inch pieces for each edge, AB and
67 CD, with a sharpie line marking the cut ends, giving us 4 samples. Then, we follow the standard scanning protocols for the
68 confocal microscope, shown in Figure 2b, to scan the wire tip surfaces. The scanned surfaces are saved in a resolution of
69 $0.645\mu m \times 0.645\mu m$ per square pixel in an x3p file format. Here, we are showing AB and CD sides in Figure 2c, with the
70 back of A being C and the back of B being D. We separate AB and CD sides into 2 pieces along the bending position, resulting
71 in 8 scans. Then, we repeated this process for all 3 locations along the blade and 5 wire cutters, with 2 replicates for each tool-
72 edge-location combination, resulting in 120 scans as our sample. Each piece was labeled following the naming conventions:

Table 1. Structure of available data and files.

	Description	Section
Raw data		
scans/	folder containing 120 topographic 3d scans corresponding to 30 aluminum wire cuts (x3p format)	Cutting Wires
meta.csv	meta information for each cut with tool, blade, and location information (CSV format)	Cutting Wires
Manual derivatives		
profiles/	folder of files with manually extracted profiles (CSV format)	Extract Profiles
Computational derivatives in the folder 'data-derived/'		
wire-signals	signals processed from corresponding profile (zipped CSV format)	Filtered Signals
wire_pairwise_ccf	CCF values of all pairwise aligned signals (zipped CSV format)	Align Signals
Image files		
pngs/	folder containing pictures of 3d scans of wire cuts (PNG format)	Cutting Wires
profile-images/	folder containing pictures of profile extracted from wire cuts (PNG format)	Extract Profiles
Visual inventory in the folder 'assessment/analysis-manual/'		
processing-wires	display of pairwise aligned signals from the same sources (HTML format)	Align Signals
Technical validation		
variability-assessment/	folder containing related documents for technical validations with the inner folder structure mimicking the structure of the main folder	Technical Validation



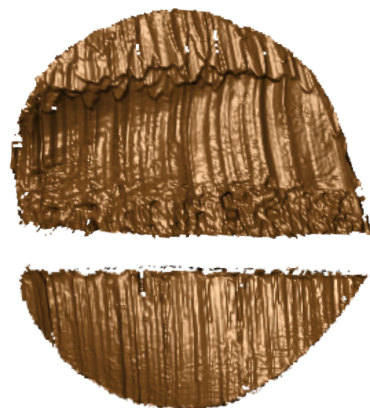
(a)

(b)

Blade A



Blade C



Blade B

Blade D

(c)

Figure 2. (a) A Kaiweets wire cutter of model KWS-105 was used to cut the wire, with inner, middle, and outer locations marked. (b) A confocal microscope was used to scan the wire-cut surfaces. (c) After separating edges by the connecting position, we obtained 4 samples - 2 samples from blade A and B, and others from blade C and D. width and height are tuned manually | full requirements see <https://www.nature.com/sdata/publish/submission-guidelines#figures>

73 T(ool) 1/2/3/4/5 (Edge) A/B/C/D W(ire) - L(ocation) I(nner)/M(iddle)/O(uter) - R(epetition) 1/2, with T1AW-LI-R1 being
 74 the piece cut by tool 1 on the A edge at the inner location for the first repetition. In order to have the sampling protocol
 75 conducted properly without mistakes, we have two team members cut and label wires together, and one of them scans in a
 76 specific order to ensure consistency across all scans, and name scans by the naming convention. In the end, we have another
 77 member checked the saved data to ensure everything was correct.

78 Extract Profiles

79 Numerical comparisons between 2 replicates cannot be done directly on the $x3p$ files. We need to extract representative
 80 functions from the scans first. A representative function with the most information is considered a signal for one scan, which
 81 is used later for comparison. To obtain this function, we first need a profile of the scan, which is a sequence of values along a
 82 user-drawn line on the surface. The profile captures most features of the scan and is orthogonal to the striation marks of the
 83 scan, which are formed by the ups and downs of grooves. So, we draw the line across the scan region to maximize the feature
 84 captured, as shown in dark blue in Figure 3a. We then investigate the values under this profile line. The profile function along
 85 the line is plotted in Figure 3b. This function still has to be processed before turning into a useful signal.

86 Filtered Signals

87 With the profile extracted, we then obtain the signal. Two Gaussian filters, as discussed in Cleveland et al.¹⁵, are applied to
 88 these resulting profiles. In particular, we first used a large low-pass filter with bandwidths of 400 microns to remove the large
 89 trend, as this trend overwhelms the signals, and then used a small high-pass filter of 40 microns to average across noise and
 90 remove spikes. Finally, the extreme tail values are removed, and the resulting signal is used for later comparison, as shown in
 91 Figure 3c.

92 Align Signals

93 After extracting signals from different scans, they are put together for comparison, and we maximize CCF values between
 94 the signals to find the best alignment numerically. We compare all possible pairs, for example, T1AW-LI-R1 to T1AW-LI-
 95 R2, which is comparing each row in Figure 4. We assume that signals from two replicates with the same tool-edge-location
 96 combination yield relatively similar signals, as in the first two columns of Figure 5, which results in alignments of massive
 97 overlapping signals and high CCF values close to 1. The alignments and values in the rightmost column of Figure 5 fulfill our
 98 expectations.

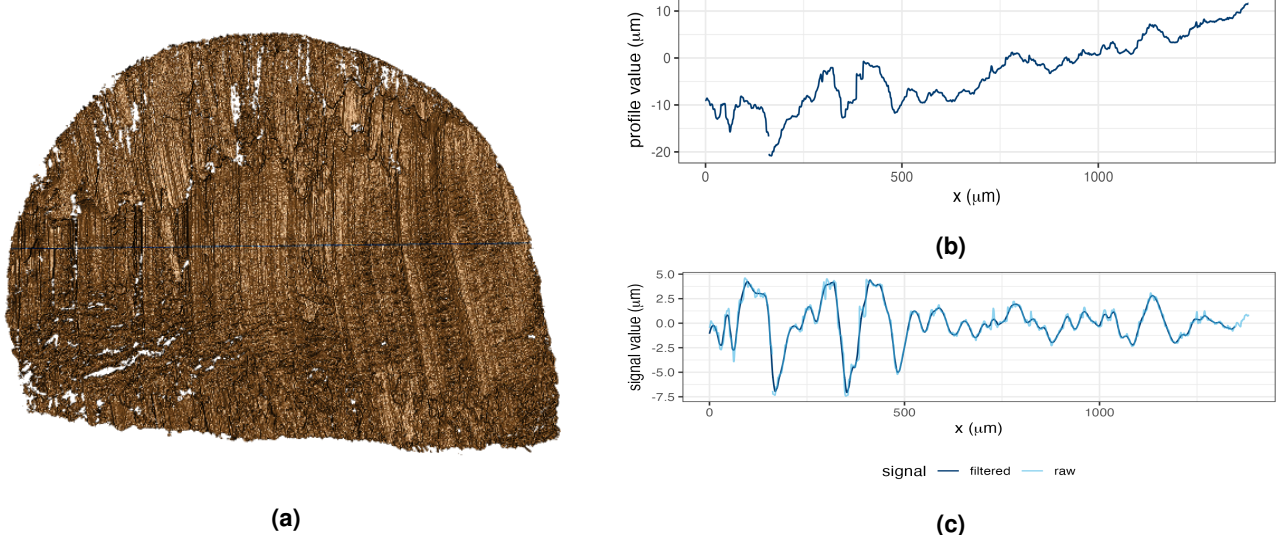


Figure 3. (a) A profile line in dark blue is drawn across the striations of the scan. (b) The profile function is extracted along the profile line in (a). (c) The raw signal in light blue is obtained by using the low-pass filter on the profile function in (b), and the filtered signal is obtained by using the high-pass filter on the raw signal.

99 Data Records

100 The complete dataset is available on the ISU DataShare repository at <https://iastate.figshare.com/>, which is public and open
101 access for every interested researcher. The structure of the dataset is described before in Table 1. need to upload when finish

102 Technical Validation

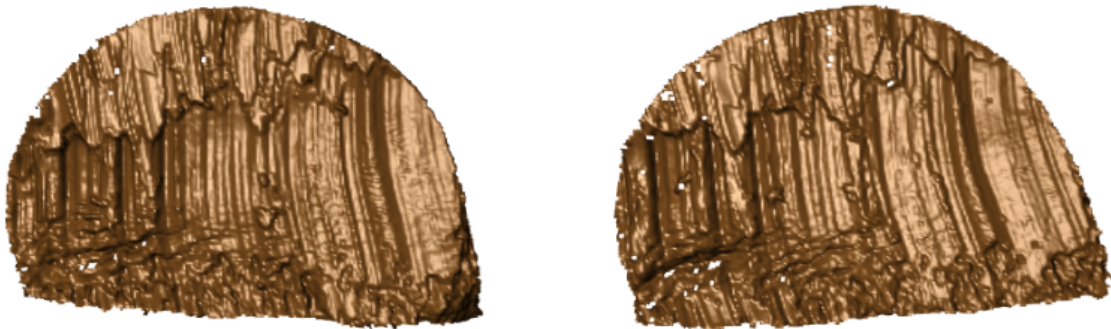
103 We conducted technical validation in different aspects, including processing and alignment of signals, and variability assessment.
104

105 The validation for processing scans and alignment of signals was conducted in the following manner. For the CCF values
106 calculated, we assume large values between signals from the same source and low scores between signals from different
107 sources. Figure 5 shown in Align Signals before matches our thought for signals from same sources. For different sources, we
108 arbitrarily take T1AW-LI-R1 and T2AW-LI-R1 as an example, as shown in Figure 6a and Figure 6b. The signal alignment is
109 shown in Figure 6c with a 0.2 CCF value, which is as low as expected. We also put resulting CCFs for all pairwise comparisons
110 in the boxplot, together with the receiver operating characteristic (ROC) curve, as in Figure 7 and Figure 8. The ROC curve
111 shows the sensitivity, or the true positive rate, against the false positive rate (FPR) (1 - specificity). This curve is very close to
112 the upper left corner, which is excellent for classification and drawing conclusions. It gives us a threshold of 0.589 to control
113 the FPR to be less than 0.05 with a false negative rate (FNR) to be 0, (false positive rate (FPR) / false discovery rate (FDR)
114 -> define the H0 or call it false identification rate (FIR)????), and 0.658 to control the FPR to be less than 0.01, with FNR to
115 be 0.02. All these results are consistent with our expectations and validate our pipeline for processing scans and alignment of
116 signals.

117 The other validation we did was to assess the variability of our pipeline. In particular, we assess the variabilities in different
118 replicates, staging, and acquisition. We arbitrarily picked scans from tool 2 at the middle location for this assessment. The
119 variability in different replicates was shown when we took two different cuts on the same edge and position, as fully discussed
120 in the previous comparison as Figure 5 shown in Align Signals. For staging, we rescanned replicate 2 under the confocal
121 microscope, introducing a new staging labeled as S in our naming protocol. All scans with staging 1 are omitted in the label,
122 resulting in R2(-S1). For all four edges of tool 2 at the middle location, we created three different stagings, R2, R2-S2, and
123 R2-S3, computed the CCF between stagings with pairwise comparison, and computed the CCF average and standard deviation
124 (SD).

125 Within each staging, we further examined the effect of different acquisitions by keeping the scans on the confocal micro-
126 scope under varying lighting conditions, introducing a new acquisition label as A. For edge A at staging 3, we performed 4
127 acquisitions in total, omitting the first one in the label again, resulting in R2-S3(-A1). For the other three edges, we conducted
128 two acquisitions in staging 3, denoted as R2-S3 and R2-S3-A2. Again, we computed the CCF between stagings with pairwise
129 comparison and the CCF average and standard deviation.

Edge A



Edge C



Edge B



Edge D



Figure 4. Scans from different sides of tool 1 at the inner location.

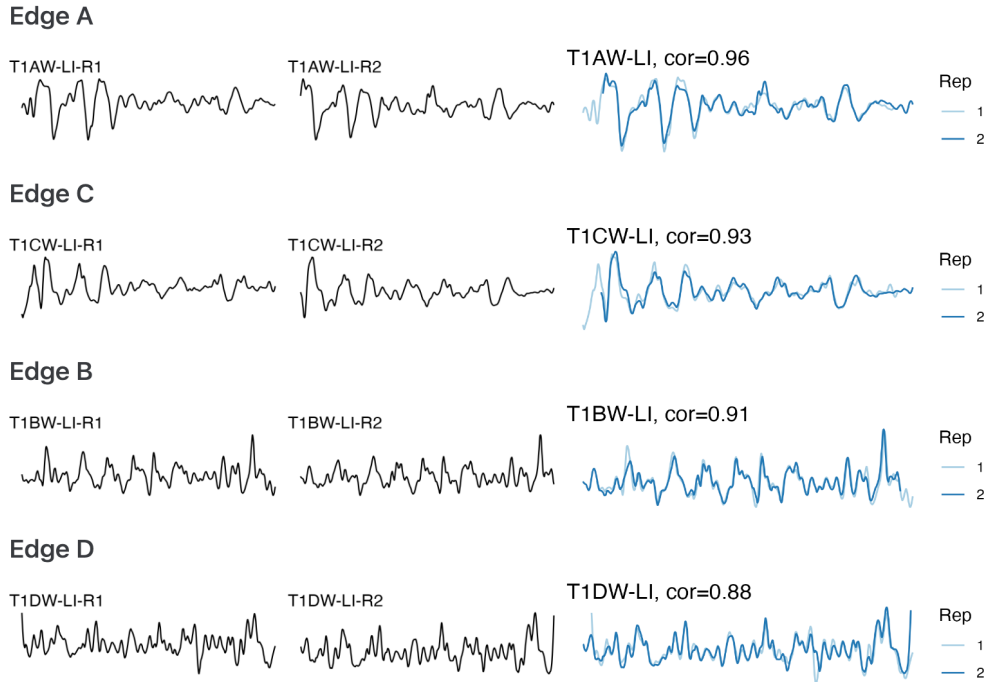


Figure 5. The first and second columns show the signals extracted from Figure 4, and the third column shows the alignments and CCF values between pairs of signals.

Table 2. Comparison of CCF means and standard deviations across different replicates, stagings, and acquisition settings.

Edge	Replicate (R)		Staging (S)			Acquisition (A)		
	Avg _R	SD _R	Avg _S	SD _S	Avg _S - Avg _R	Avg _A	SD _A	Avg _A - Avg _S
A	0.818	0.015	0.961	0.012	0.143	0.992	0.003	0.031
B	0.879	0.031	0.922	0.042	0.043	0.939	—	0.017
C	0.841	0.022	0.952	0.021	0.111	0.959	—	0.007
D	0.797	0.011	0.966	0.017	0.169	0.986	—	0.020

With this setup, we expect an increasing consistency in the CCF from replicate to staging to acquisition as conditions become progressively more stable when scanning. Consequently, variability should decrease along this sequence. We also computed the differences between replicate, staging, and acquisition, expecting more minor differences between acquisition and staging than between staging and replicate. We visualized the results as scatter plots, as shown in Figure 9. The interval within 2 standard deviations is also shown. There is an increase in the average, as shown in higher orange bars, and a decrease in standard deviation, as shown in the shorter interval width in the plot. The detailed numeric results, including means, standard deviation, and differences in averages, are shown in Table 2, confirming our expectations.

One thing to note is that our variability assessment does not include variability in the CCFs due to differences in manually extracting profiles from scans. For the purpose of reproducibility of the results stated here, we have included the extraction location and values for each scan.

Usage Notes

The R package `x3ptools`¹⁶ available from CRAN supports working with files in `x3p` format. The sample scripts in R for processing scans from `x3p` format to their signal and alignment are available on GitHub [heike/wirecuts-data](#) in the assessment/code folder, as described in Table 3.

We already conduct pairwise comparisons and visualize some of the comparison results in Align Signals and Technical Validation. Here, we introduce some other analysis plots. Suppose we put the CCF values in a tilemap with different tools, locations, and edge combinations. In that case, we expect only the diagonal to have high CCF values, close to 1 and marked

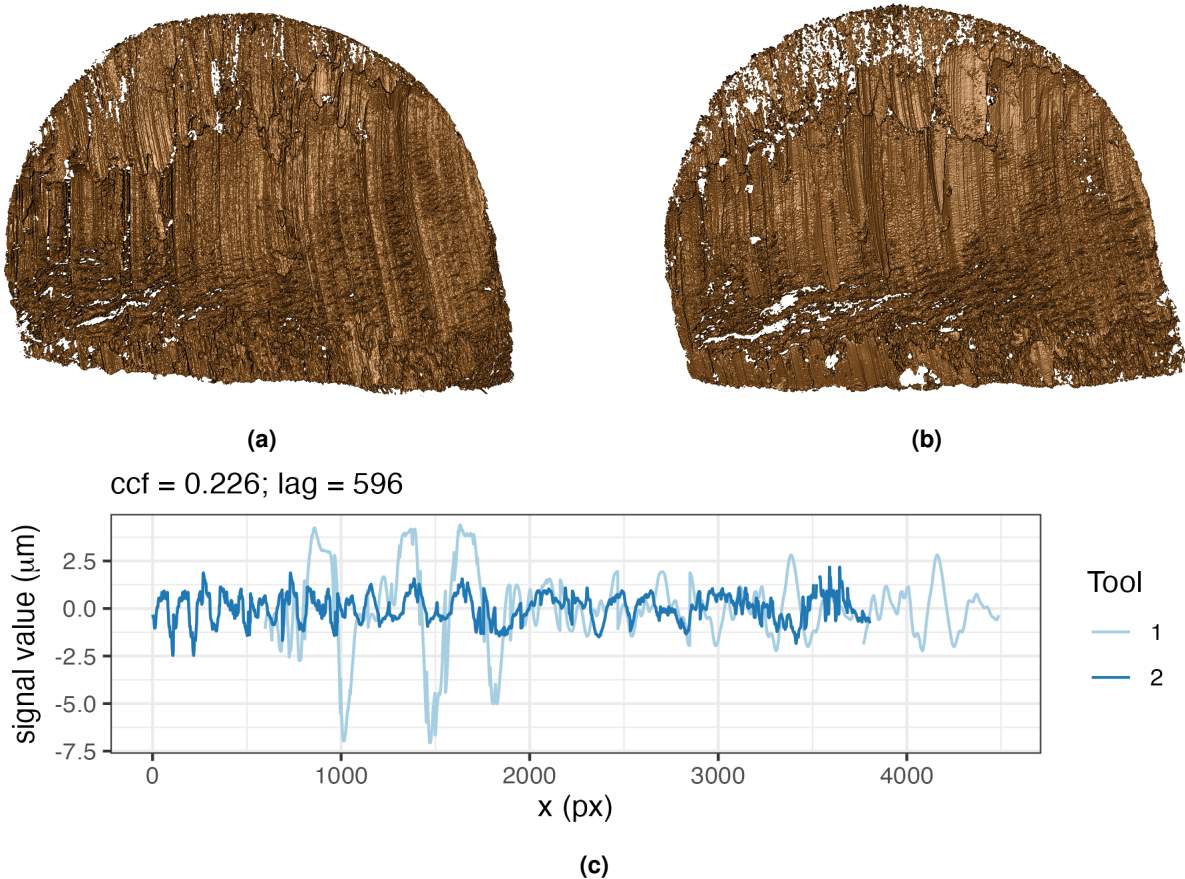


Figure 6. (a) Scan T1AW-LI-R1 cut by tool 1. (b) Scan T2AW-LI-R1 cut by tool 2. (c) Alignment of signals from T1AW-LI-R1 and T2AW-LI-R1.

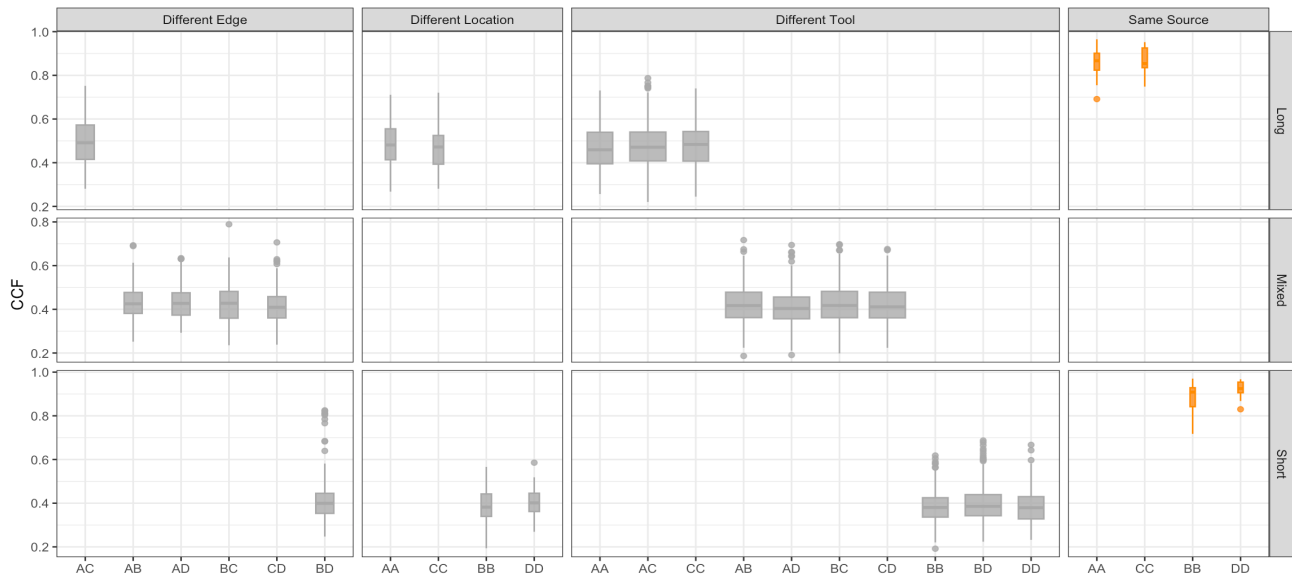


Figure 7. The boxplot shows that signals from the same sources have higher CCFs than those from different sources.

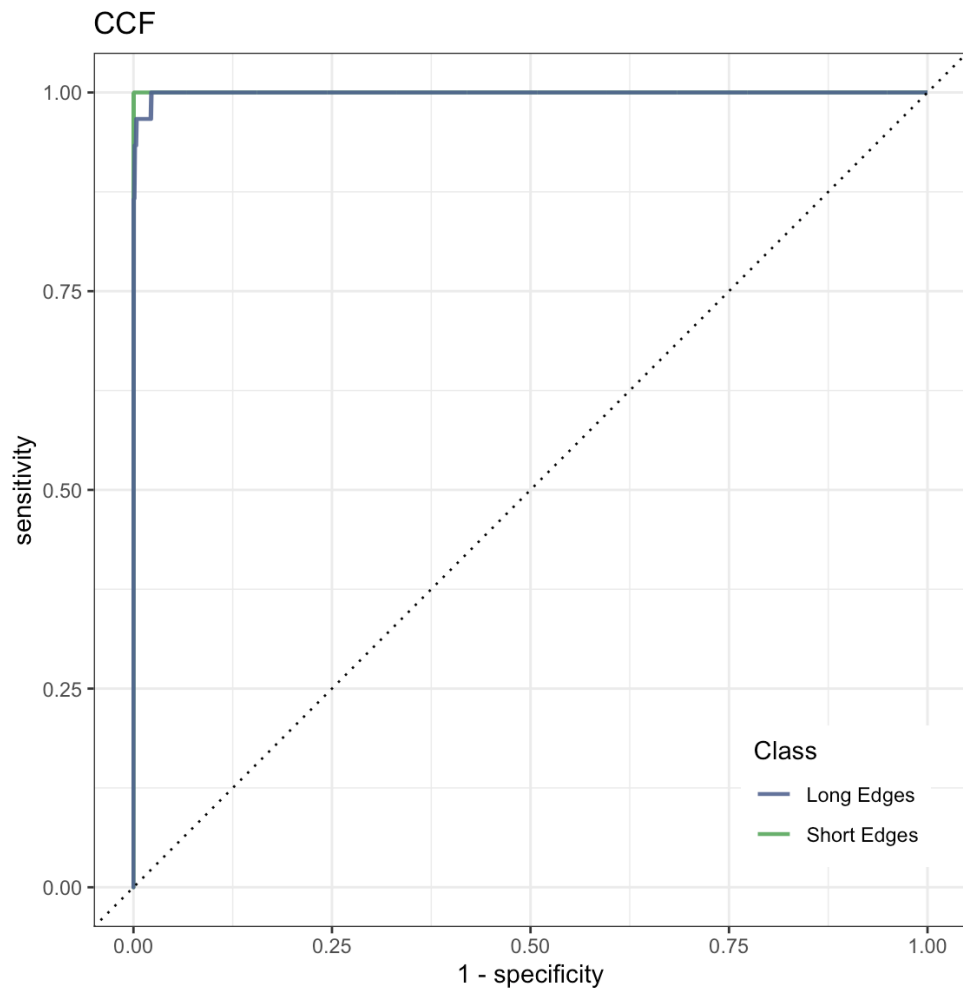


Figure 8. The ROC curve is bending very close to the upper left corner, which means excellent in classification and drawing conclusions.

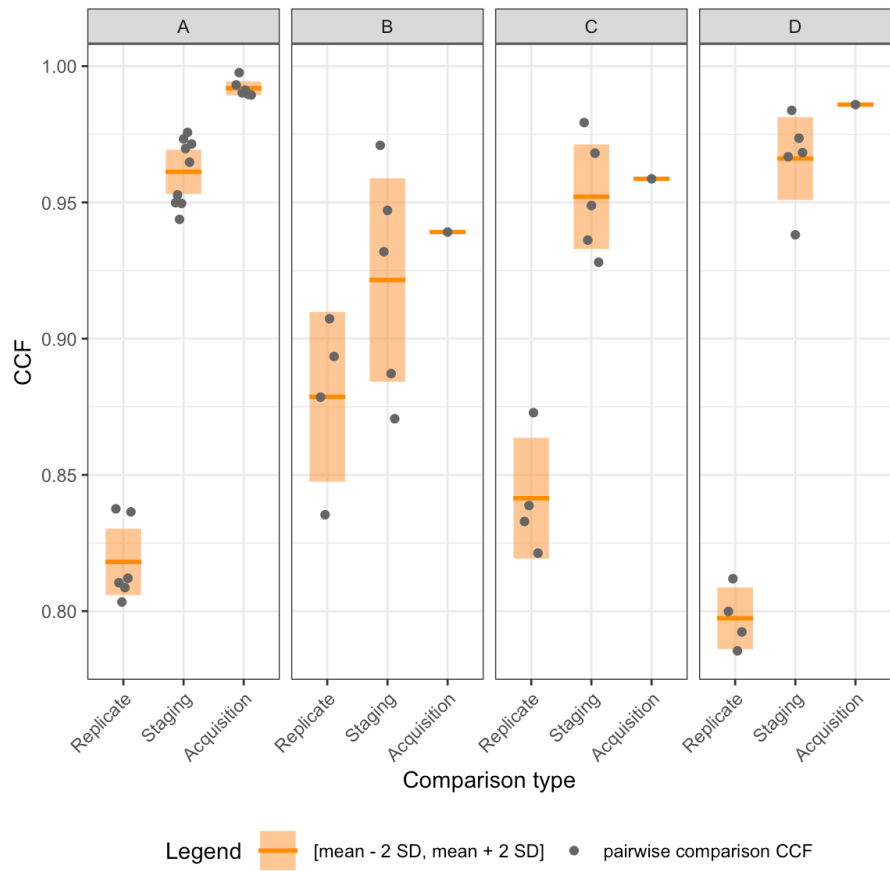


Figure 9. Scatter plots of CCF under different replicate, staging, and acquisition conditions with means and 2 standard deviation intervals.

Table 3. Overview of available codes.

	Description	Section
Inspect raw scans		
1-create_pngs_from_x3p.R	obtain images of x3ps in scans /	Cutting Wires
Extract profiles		
2-create_profiles_from_x3p.R	manually extract profiles from each scan	Extract Profiles
3-create-single-profile-file.R	create meta profile information	Extract Profiles
Derive signals		
4-create_signals_from_profiles.R	derive signals from each profile	Filtered Signals
Align signals		
5-create-images.R	create images for pairwise alignment	Align Signals
6-align-pairwise.R	compute pairwise alignment CCF values	Align Signals
7-all-comparison-results.R	visualize comparison results	Align Signals

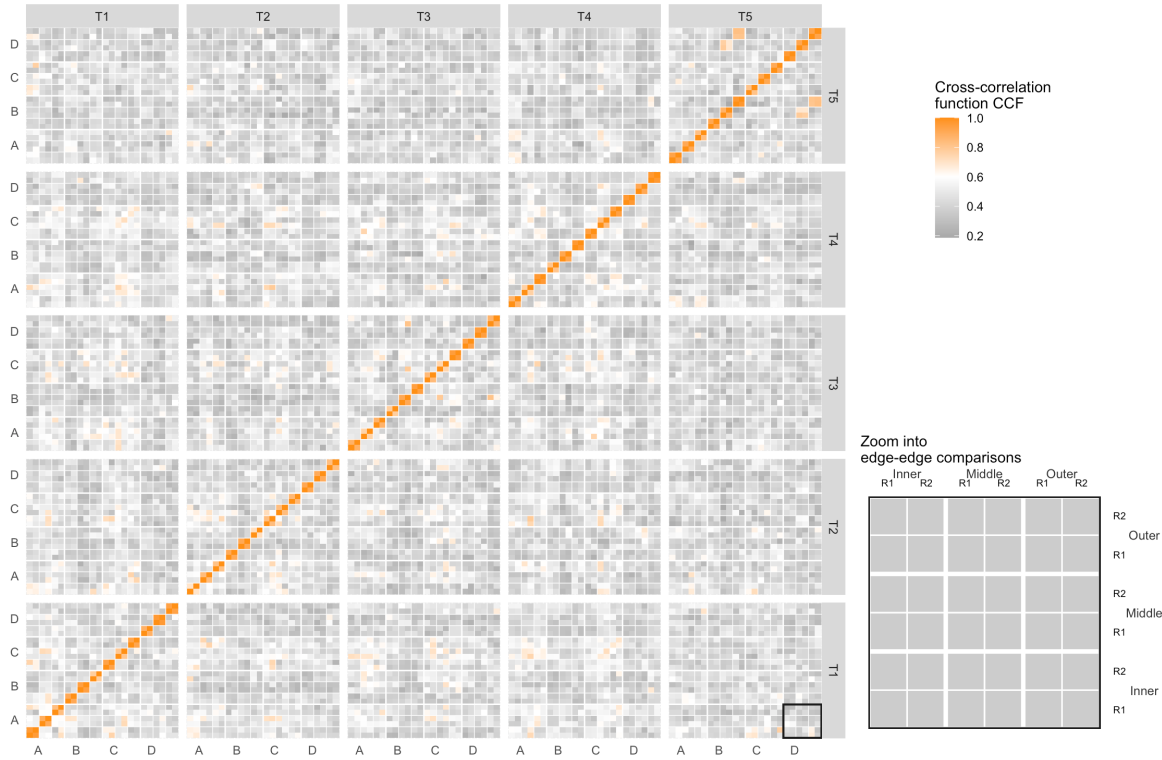


Figure 10. The tilemap shows signals from the same source have CCFs close to 1.

as orange in the tilemap, as the diagonal represents the same source, and the rest of the matrix to have low CCF values, close to 0 and marked as gray. In Figure 10, the behavior is consistent with our expectation overall, except for some rare cases with tool 5 edge D. The density plot in Figure 11 shows the distribution of the CCF values with the same sources and different sources. The overlapping points between the tails of these two distributions are a rough threshold for drawing conclusions.

Code availability

We made available all codes we used for inspecting raw scans, extracting profiles, deriving signals, aligning signals, and visualizing comparison results discussed in [Methods](#) and [Technical Validation](#), as described in Table 3. All results are reproducible using these codes provided.

References

1. Lindley, D. V. A Problem in Forensic Science. *Biometrika* **64**, 207, [10.2307/2335686](https://doi.org/10.2307/2335686) (1977). [2335686](https://doi.org/10.2307/2335686).
2. AFTE. The association of firearm and tool mark examiners: Theory of identification as it relates to toolmarks. *AFTE J.* **30**, 86–88 (1998).
3. NRC. *National Research Council: Strengthening Forensic Science in the United States: A Path Forward* (National Academies Press, 2009).
4. President's Council of Advisors on Science and Technology. *President's Council of Advisors on Science and Technology: Forensic Science in Criminal Courts: Ensuring Scientific Validity of Feature-Comparison Methods* (Executive Office of the President of the United States, President's Council, Washington, D.C., 2016).
5. Biedermann, A. The strange persistence of (source) “identification” claims in forensic literature through descriptivism, diagnosticism and machinism. *Forensic Sci. Int. Synerg.* **4**, 100222, [10.1016/j.fsisyn.2022.100222](https://doi.org/10.1016/j.fsisyn.2022.100222) (2022).
6. Baiker, M., Pieterman, R. & Zoon, P. Toolmark variability and quality depending on the fundamental parameters: Angle of attack, toolmark depth and substrate material. *Forensic Sci. Int.* **251**, 40–49, [10.1016/j.forsciint.2015.03.003](https://doi.org/10.1016/j.forsciint.2015.03.003) (2015).

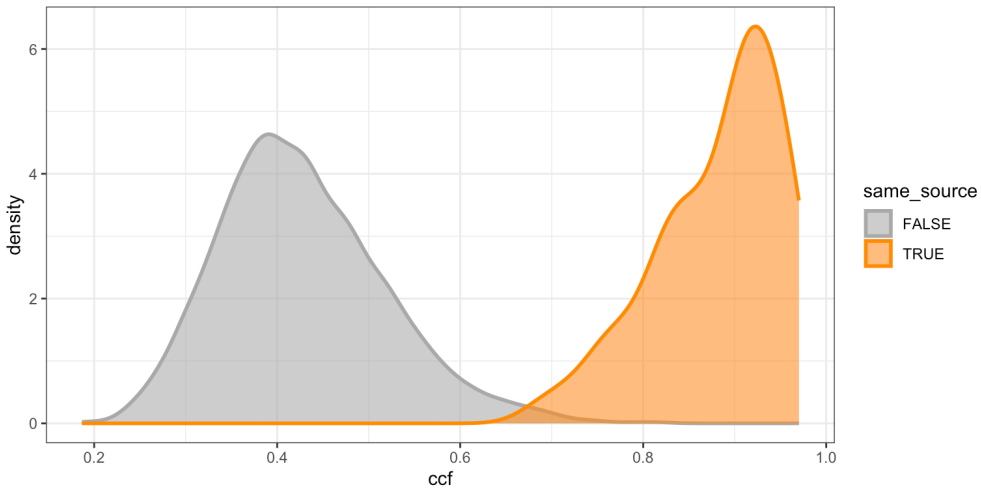


Figure 11. The density plot shows tails of distributions overlap, which to be used as a rough threshold for drawing conclusions.

- 168 7. Garcia, D. L., Pieterman, R. & Baiker, M. Influence of the axial rotation angle on tool mark striations. *Forensic Sci. Int.*
169 **279**, 203–218, [10.1016/j.forsciint.2017.08.021](https://doi.org/10.1016/j.forsciint.2017.08.021) (2017).
- 170 8. Cuellar, M., Gao, S. & Hofmann, H. An algorithm for forensic toolmark comparisons. *Forensic Sci. Int. Synerg.* **9**,
171 100543, [10.1016/j.fsisy.2024.100543](https://doi.org/10.1016/j.fsisy.2024.100543) (2024).
- 172 9. Ma, L. *et al.* NIST Bullet Signature Measurement System for RM (Reference Material) 8240 Standard Bullets. *J. Forensic
173 Sci.* **49**, 1–11, [10.1520/JFS2003384](https://doi.org/10.1520/JFS2003384) (2004).
- 174 10. Zheng, X. A., Soons, J. A. & Thompson, R. M. NIST Ballistics Toolmark Research Database | NIST (2016).
- 175 11. Chu, W., Thompson, R. M., Song, J. & Vorburger, T. V. Automatic identification of bullet signatures based on consecutive
176 matching striae (CMS) criteria. *Forensic Sci. Int.* **231**, 137–141, [10/gn65cz](https://doi.org/10/gn65cz) (2013).
- 177 12. Vorburger, T. *et al.* Applications of cross-correlation functions. *Wear* **271**, 529–533, [10.1016/j.wear.2010.03.030](https://doi.org/10.1016/j.wear.2010.03.030) (2011).
- 178 13. Hare, E., Hofmann, H., Carriquiry, A. *et al.* Automatic matching of bullet land impressions. *The Annals Appl. Stat.* **11**,
179 2332–2356, [10.1214/17-AOAS1080](https://doi.org/10.1214/17-AOAS1080) (2017).
- 180 14. Ju, W. & Hofmann, H. The R Journal: An Open-Source Implementation of the CMPS Algorithm for Assessing Similarity
181 of Bullets. *The R J.* **14**, 267–285, [10.32614/RJ-2022-035](https://doi.org/10.32614/RJ-2022-035) (2022).
- 182 15. Cleveland, W. S., Grosse, E. & Shyu, W. M. Local Regression Models. In *Statistical Models in S* (Routledge, 1992).
- 183 16. Hofmann, H., Vanderplas, S., Krishnan, G. & Hare, E. X3ptools: Tools for Working with 3D Surface Measurements,
184 [10.32614/CRAN.package.x3ptools](https://doi.org/10.32614/CRAN.package.x3ptools) (2018).

185 Acknowledgements

186 This work was partially funded by the Center for Statistics and Applications in Forensic Evidence (CSAFE) through Cooper-
187 ative Agreement 70NANB20H019 between NIST and Iowa State University, which includes activities carried out at Carnegie
188 Mellon University, Duke University, University of California Irvine, University of Virginia, West Virginia University, Univer-
189 sity of Pennsylvania, Swarthmore College and the University of Nebraska-Lincoln.

190 **Author contributions statement**

191 Let's follow the Elsevier definitions: <https://www.elsevier.com/researcher/author/policies-and-guidelines/credit-author-statement>
192 Y.L.: Methodology, Software, Validation, Data Curation, Writing - Draft; H.H.: Conceptualization, Methodology, Valida-
193 tion, Writing - Review & Editing; C.M.: Lab supervision; E.A.: Physical Specimen, Scanning; J.S: Forensic advice; A.C.:
194 Funding acquisition.
195 All authors reviewed the manuscript.

196 **Competing interests**

197 (mandatory statement)

198 H.H. is a technical advisor to AFTE (Association of Firearms and Toolmarks Examiners), fellow of the ASA (American
199 Statistical Association), and committee member of the ASA Forensic Science Committee. H.H. has testified as court witness
200 on behalf of judge April Neubauer, NY State Supreme Court Criminal Term in New York City. [other competing interests -](#)
201 [Alicia?](#)